

E-Beam Interaction with Plasmas in a Coaxial Irised Slow-Wave Transmission Line

G.V. Sotnikov

Kharkov Institute of Physics and Technology
st. Akademicheskaya 1, 61108 Kharkov, Ukraine
e-mail: sotnikov@kipt.kharkov.ua

Contents

1. Introduction	71
2. Linear Operation Mode	72
3. Non-Linear Operation Mode	76
4. Conclusions	78

Abstract

A theoretical study is made on electron beam-excited microwave oscillations in a coaxial transmission line, with combs placed on the inner and outer conductors. The transit channel of the structure, where an annular e-beam propagates, is filled up with plasma. Eigen waves in the coaxial plasma-filled line are studied as well as their relationship vs. plasma density. Plasma is shown to cause a considerable increase in the gain, broadening concurrently the excited oscillation spectrum. The non-linear analysis is made of oscillation amplification. Determined are the maximum longitudinal electric field amplitude and coupling efficiency for different plasma densities. Comparison of the above characteristics with similar ones for the vacuum structure points out superiority of the plasma-filled hybrid structure over the vacuum structure.

1. Introduction

The vacuum slow-wave structure (SWS) can acquire the well-known hybrid features after filling the interaction area (transit channel for electron beam to travel in) with plasma. The principles of hybrid plasma SWS were laid down for the first time in the papers [1, 2]. As a result of the transit channel filling with plasma, the electric field longitudinal component increases strongly, causing the coupling coefficient and, consequently, wave gain to increase. In so doing, if such conditions are realized when a coupling with the vacuum structure eigen waves takes place, a high amount of microwave power is generated. Experimental studies [3-5] supported the theoretical predictions of promise in hybrid SWS as a base of high-power amplifiers and generators.

It should be reminded that the pioneering research on hybrid plasma structures was done, using vacuum SWS of the coupled cavity chain type. The conditions for microwave oscillation generation in such a hybrid structure are optimum when the oscillating

synchronous frequency is equal to the plasma one. In this way, a narrow oscillation spectrum (on the order of increment) is excited for a given plasma density. The authors in the paper [6] put forward a suggestion that during filling of the vacuum structure, in which the slow cable wave exists in a broad pass band, plasma might be able to retain a wide oscillation amplification bandwidth, increasing concurrently the gains.

This paper studies the amplitude-frequency characteristics (AFC) of an amplifier, based on the coaxial irised transmission line, with irises placed on the inner and outer cylinders and the transit channel filled with plasma. The linear and non-linear pulse amplification theories, based on the vacuum structure, were reported at the conferences "Crimico'97-[7], "Beams'98", published in their proceedings and [9]. This structure was demonstrated to be really capable of microwave generation across a broad frequency range. Below, the studies will be presented on variations of the dispersion characteristics, gains and oscillation amplitudes as a result of filling the coaxial slow-wave transmission line transit

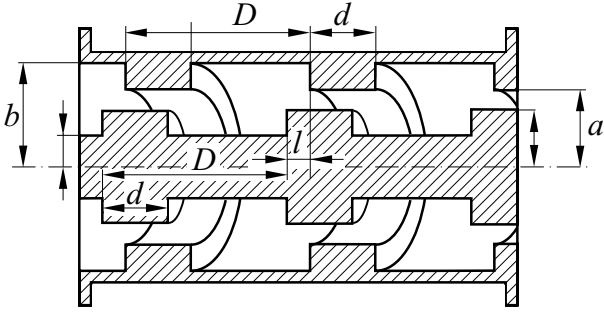


Fig. 1. Sketch of the coaxial SWS.

channel with plasma. Note that the authors [6] made preliminary studies on the gains and coupling coefficients in a plasma-filled coaxial transmission line with disks placed on the inner conductor. Plasma was demonstrated to change drastically the SWS electro-dynamic characteristics if the transit channel transverse size is comparable with the amplified oscillation wavelength or exceeds it. This observation is conditioned by the resonance wave surface nature (consideration is given to e-beam interaction with the zero spatial harmonic of the cable mode). Plasma changes the picture cardinally only in the case of high plasma densities.

2. Linear Operation Mode

The SWS under consideration (Fig. 1) is a coaxial transmission line with the inner and outer cylinder radii ρ and b , respectively, and disks on both conductors. Plasma with the density n_p fills up the transit channel with the inner σ and outer a radii. A thin electron beam propagates through this channel with its radius being r_b , velocity v_0 , current I_b . The structure period is D , with the cavity width being the same and equal to d . The inner structure can be shifted relative to the outer one at an arbitrary distance l .

In the linear approximation, the dispersion equation, describing the monochromatic wave excitation by e-beam, can be obtained via the partial area method. In this case, let us break down conditionally the SWS into four areas: $I - a \leq r \leq b$, $II_{<} - \sigma \leq r \leq r_b$, $II_{>} - r_b \leq r \leq a$, $III - \rho \leq r \leq \sigma$. In each area, one must find solution of the Maxwell equations with the accuracy as high as arbitrary constants and join them all together on the common boundaries. Owing to the periodicity of the SWS, perturbations of all values in the transit channel have the relationship

$$X = \sum_{m=-\infty}^{m=\infty} X_m \exp(i\beta_m z - i\omega t), \quad (1)$$

where $\beta_m = \beta_0 + 2\pi m/D$, ω is the wave frequency, the axis z is directed along the structure. We shall

confine ourselves to the standing wave fundamental spatial harmonic in the cavity region. The boundary conditions consist in the zero electric field tangential components on metallic surfaces, continuity of the tangential components of electric and magnetic fields on the interface boundary between the transit channel and cavities. The in-beam components of the electric E_r and magnetic H_φ fields undergo such rupture stress, the value of which is proportional to the beam current:

$$H_{\varphi,m}^{II_{>}} - H_{\varphi,m}^{II_{<}} = i \frac{2e\omega I_b}{(\omega - \beta_m v_0)^2 \gamma_0^3 m c v_0 r_b} E_{z,m}(r_b) \quad (2)$$

where $\gamma_0 = 1/\sqrt{1 - v_0^2/c^2}$.

In order to improve convergence of the method, one must take into account the quasi-static tangential electric field property near the iris acute angles [10,12]:

$$E_z^I = E_z^{II_{<}}|_{r=a} = \begin{cases} M_1, & |z + nD| < d/2, \\ 0, & d/2 < |z + nD| < D/2, \end{cases} \quad (3)$$

$$E_z^{III} = E_z^{II_{>}}|_{r=\sigma} = \begin{cases} M_2 \exp(i\beta_0 l), & |z - l + nD| < d/2, \\ 0, & d/2 < |z - l + nD| < D/2, \end{cases} \quad (4)$$

The expressions (3)-(4) assume that the longitudinal coordinate $z = 0$ corresponds to the mid-part of the internal resonator, M_1 and M_2 are the arbitrary constants, n is the integer, determining the cavity number.

As a result of the electric field longitudinal component boundary $r = \sigma$, $r = \sigma$ joining and acting in consideration of (3)-(4) and the in-beam limiting conditions (2), we shall obtain the expressions for E -wave electromagnetic field components in the partial areas:

$$E_z^I = M_1 \frac{F_0(k, r, b)}{F_0(k, a, b)}, \quad H_\varphi^I = -iM_1 \frac{F_1(k, r, b)}{F_0(k, a, b)}, \quad (5)$$

$$E_z^{III} = M_2 \exp(i\beta_0 l) \frac{F_0(k, r, \rho)}{F_0(k, \sigma, \rho)} \quad (6)$$

$$H_\varphi^I = -iM_2 \exp(i\beta_0 l) \frac{F_0(k, r, \rho)}{F_0(k, \sigma, \rho)}$$

$$E_z^{II_{>}} = \frac{d}{D} \sum_{m=-\infty}^{\infty} \frac{\Psi_m}{\Delta_m} \exp(i\beta_m z) \left\{ M_2 \exp(-im\varphi_0) \times \frac{F_0(k_{\perp m}, r, a)}{F_0(k_{\perp m}, \sigma, a)} + M_1 \left[\frac{F_0(k_{\perp m}, r, \sigma)}{F_0(k_{\perp m}, a, \sigma)} - \frac{\alpha_m^2 F_0(k_{\perp m}, r, r_b) F_0(k_{\perp m}, r_b, \sigma)}{(\omega - \beta_m v_0)^2 F_0(k_{\perp m}, a, \sigma)} \right] \right\}, \quad (7)$$

$$H_{\varphi}^{II>} = \frac{d}{D} \sum_{m=-\infty}^{\infty} \frac{-ik\varepsilon_3}{k_{\perp m}} \frac{\Psi_m}{\Delta_m} \times \exp(i\beta_m z) \left\{ M_2 \exp(-im\varphi_0) \frac{F_1(k_{\perp m}, r, a)}{F_0(k_{\perp m}, \sigma, a)} + M_1 \left[\frac{F_1(k_{\perp m}, r, \sigma)}{F_0(k_{\perp m}, a, \sigma)} - \frac{\alpha_m^2 F_1(k_{\perp m}, r, r_b)}{(\omega - \beta_m v_0)^2} \times \frac{F_0(k_{\perp m}, r_b, \sigma)}{F_0(k_{\perp m}, a, \sigma)} \right] \right\}, \quad (8)$$

$$E_r^{II>} = \frac{d}{D} \sum_{m=-\infty}^{\infty} \frac{-i\beta_m \varepsilon_3}{k_{\perp m}} \frac{\Psi_m}{\Delta_m} \times \exp(i\beta_m z) \left\{ M_2 \exp(-im\varphi_0) \frac{F_1(k_{\perp m}, r, a)}{F_0(k_{\perp m}, \sigma, a)} + M_1 \left[\frac{F_1(k_{\perp m}, r, \sigma)}{F_0(k_{\perp m}, a, \sigma)} - \frac{\alpha_m^2 F_1(k_{\perp m}, r, r_b)}{(\omega - \beta_m v_0)^2} \times \frac{F_0(k_{\perp m}, r_b, \sigma)}{F_0(k_{\perp m}, a, \sigma)} \right] \right\}, \quad (9)$$

$$E_z^{II<} = \frac{d}{D} \sum_{m=-\infty}^{\infty} \frac{\Psi_m}{\Delta_m} \exp(i\beta_m z) \left\{ M_1 \frac{F_0(k_{\perp m}, r, \sigma)}{F_0(k_{\perp m}, a, \sigma)} + M_2 \exp(-im\varphi_0) \left[\frac{F_0(k_{\perp m}, r, a)}{F_0(k_{\perp m}, \sigma, a)} - \frac{\alpha_m^2 F_0(k_{\perp m}, r, r_b)}{(\omega - \beta_m v_0)^2} \frac{F_0(k_{\perp m}, r_b, a)}{F_0(k_{\perp m}, \sigma, a)} \right] \right\}, \quad (10)$$

$$H_{\varphi}^{II<} = \frac{d}{D} \sum_{m=-\infty}^{\infty} \frac{-ik\varepsilon_3}{k_{\perp m}} \frac{\Psi_m}{\Delta_m} \times \exp(i\beta_m z) \left\{ M_1 \frac{F_1(k_{\perp m}, r, \sigma)}{F_0(k_{\perp m}, a, \sigma)} + M_1 \exp(-im\varphi_0) \left[\frac{F_1(k_{\perp m}, r, a)}{F_0(k_{\perp m}, \sigma, a)} - \frac{\alpha_m^2 F_1(k_{\perp m}, r, r_b)}{(\omega - \beta_m v_0)^2} \frac{F_0(k_{\perp m}, r_b, a)}{F_0(k_{\perp m}, a, \sigma)} \right] \right\}, \quad (11)$$

$$E_r^{II<} = \frac{d}{D} \sum_{m=-\infty}^{\infty} \frac{-i\beta_m \varepsilon_3}{k_{\perp m}} \frac{\Psi_m}{\Delta_m} \times \exp(i\beta_m z) \left\{ M_1 \frac{F_1(k_{\perp m}, r, \sigma)}{F_0(k_{\perp m}, a, \sigma)} + M_2 \exp(-im\varphi_0) \left[\frac{F_1(k_{\perp m}, r, a)}{F_0(k_{\perp m}, \sigma, a)} - \frac{\alpha_m^2 F_1(k_{\perp m}, r, r_b)}{(\omega - \beta_m v_0)^2} \frac{F_0(k_{\perp m}, r_b, a)}{F_0(k_{\perp m}, a, \sigma)} \right] \right\}, \quad (12)$$

In the expressions (7)-(12) the sign ">" stands to mean that the field expressions are true at $r > r_b$, with the sign "<" meaning the same at $r < r_b$; the remaining designations have the following form:

$$\begin{aligned} F_n(q, x, y) &= J_n(qx)Y_0(qy) - Y_n(qx)J_n(qy), \\ \varepsilon_3 &= 1 - \omega_p^2, \quad \omega_p^2 = 2\pi e^2 n_p / m, \\ k_{\perp m} &= \sqrt{(k^2 - \beta_m^2) \varepsilon_3}, \quad k = \omega / c, \\ \varphi_0 &= 2\pi l / D, \quad \Psi_m = \sin(\beta_m d / 2) / (\beta_m d / 2), \\ \Delta_m &= 1 + \frac{\alpha_m^2 F_0(k_{\perp m}, r_b, a)}{(\omega - \beta_m v_0)^2} \frac{F_0(k_{\perp m}, r_b, \sigma)}{F_0(k_{\perp m}, \sigma, a)}, \\ \alpha_m^2 &= \frac{I_b}{I_A} \frac{\pi c^3 (k^2 - \beta_m^2)}{\gamma_0^3 v_0}, \quad I_A = 17kA, \end{aligned}$$

J_n, Y_n - are the Bessel and Weber functions of the n -th order.

The requirement for microwave power radial flow continuity at the transit channel interface is exactly what leads up to the sought dispersion equation:

$$Y_{12}Y_{32} - Y_{11}Y_{33} = 0, \quad (13)$$

$$Y_{12} = \frac{d}{D} \sum_{m=-\infty}^{\infty} \frac{k\varepsilon_3}{k_{\perp m}} \frac{\Psi_m^2}{\Delta_m} \left[\frac{F_1(k_{\perp m}, a, \sigma)}{F_0(k_{\perp m}, a, \sigma)} - \frac{\alpha_m^2}{(\omega - \beta_m v_0)^2} F_1(k_{\perp m}, a, r_b) \times \frac{F_0(k_{\perp m}, r_b, \sigma)}{F_0(k_{\perp m}, a, \sigma)} \right] - \frac{F_1(k, a, b)}{F_0(k, a, b)}, \quad (14)$$

$$Y_{32} = \frac{d}{D} \sum_{m=-\infty}^{\infty} \frac{k\varepsilon_3}{k_{\perp m}} \frac{\Psi_m^2}{\Delta_m} \left[\frac{F_1(k_{\perp m}, \sigma, a)}{F_0(k_{\perp m}, \sigma, a)} - \frac{\alpha_m^2}{(\omega - \beta_m v_0)^2} F_1(k_{\perp m}, \sigma, r_b) \times \frac{F_0(k_{\perp m}, r_b, a)}{F_0(k_{\perp m}, \sigma, a)} \right] - \frac{F_1(k, \sigma, \rho)}{F_0(k, \sigma, \rho)}, \quad (15)$$

$$Y_{11} = \frac{d}{D} \sum_{m=-\infty}^{\infty} \frac{k\varepsilon_3}{k_{\perp m}} \frac{\Psi_m^2}{\Delta_m} \times \exp(im\varphi_0) \frac{F_1(k_{\perp m}, a, a)}{F_0(k_{\perp m}, \sigma, a)}, \quad (16)$$

$$Y_{33} = \frac{d}{D} \sum_{m=-\infty}^{\infty} \frac{k\varepsilon_3}{k_{\perp m}} \frac{\Psi_m^2}{\Delta_m} \times \exp(-im\varphi_0) \frac{F_1(k_{\perp m}, \sigma, \sigma)}{F_0(k_{\perp m}, a, \sigma)}, \quad (17)$$

Y_{12} and Y_{32} have a clear physical sense. They describe eigen oscillations of the SWS with irises placed on the outer ($Y_{12} = 0$) and inner ($Y_{32} = 0$) conductors. The dispersion equation derivation procedure allows to

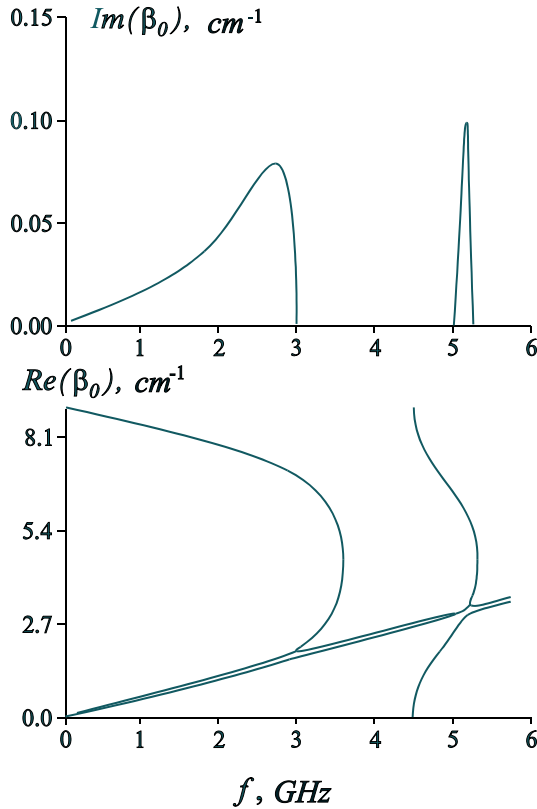


Fig. 2. Real ($Re\beta_0$) and imaginary ($Im\beta_0$) parts of the longitudinal wave number of the beam-running vacuum coaxial SWS as a function of frequency. Parameters of the structure: $b = 5.3$ cm, $a = 4.0$ cm, $\sigma = 3.5$ cm, $\rho = 1.9$ cm, $D = 0.7$ cm, $d = 0.5$ cm, $\varphi_0 = 0$, $r_b = 3.6$ cm, beam current $I_b = 5.0$ A, energy $W_b = 35$ keV.

associate the arbitrary constants M_1 and M_2 between themselves:

$$M_2 = -\frac{M_1 Y_{12}}{Y_{11}} \text{ or } M_2 = -\frac{M_1 Y_{33}}{Y_{32}}. \quad (18)$$

The numerical solution of the equation (13) was made for such parameters of the structure and beam that were used in an experiment, carried out at NSC/KIPT [11]: $b = 5.3$ cm, $a = 4.0$ cm, $\sigma = 3.5$ cm, $\rho = 1.9$ cm, $D = 0.7$ cm, $d = 0.5$ cm, $\varphi_0 = 0$, $r_b = 3.6$ cm, $I_b = 5.0$ A, $W_b = 35$ keV. The dispersion curves are presented for subsequent comparison in Fig. 2 of the SWS vacuum part. The plots, shown in Fig. 2, are presented as relationships of the real $Re\beta_0$ and imaginary $Im\beta_0$ parts of the longitudinal wave number vs. frequency $f = \omega/2\pi$. In the frequency range $f = 0 \div 5.3$, the SWS has two pass bands: a low-frequency one $f = 0 \div 3.6$ GHz with the dispersion that is similar to that in the spiral SWS [13,14] and such phase velocity, that is determined in the low frequency region by the expression $v_{ph}/c =$

$$\sqrt{\frac{\ln(a/\sigma)}{\ln(a/\sigma) + d \ln(b\sigma/a\rho)/D}}, \text{ and a high- frequency}$$

one $f = 4.5 \div 5.3$ GHz. The low frequency pass band cut-off frequency is determined in this case by such an internal SWS that has high irises, with the upper high-frequency pass band cut-off frequency being determined by the external comb. This circumstance must be taken into account while using thin (that do not fill up the transit channel) e-beams in order to generate eigen oscillations of the structure. The beam must be placed nearer to the structure that determines the eigen wave. It must be noted that the two above pass bands exist simultaneously only in the case of a two-comb slow-wave line. If there is one external, or one internal, SWS, then only the coaxial wave with the upper cut-off frequency, determinable by the cavity transverse dimensions, is present. The imaginary part in the relationship of the longitudinal wave number $Im\beta_0$ vs. frequency also has two characteristic ranges. The first one determines the coaxial slow wave enhancement in the range $f = 0 \div 3$ GHz (amplification band is narrower than pass band). The gain-vs.-frequency relationship has a peak in the vicinity of the beam resonance interactions with the eigen wave structure, then it decreases linearly to the low-frequency region and terminates steeply up into the high-frequency region. The second sharp and narrow peak is determined by beam resonance with the eigen wave of the pass band structure that follows up next. The group velocity of this wave is considerably lower than the coaxial slow wave group velocity, and for this reason the maximum gain is nearly three times that of the first range. Yet, the resonance width is considerably narrower than in the first range.

Fig. 3 shows dispersion relationships of a plasma-filled SWS ($n_p = 1.8 \cdot 10^{11} \text{ cm}^{-3}$). This plasma density corresponds to the case when the plasma frequency $f_p = \omega_p/2\pi$ overlaps the upper coaxial mode cut-off frequency. In addition to the waves, existing in a vacuum SWS, a great number of waves has appeared that corresponds to various radial and Floquet-harmonics of the coaxial plasma column eigen oscillations. If the beam resonance interactions are in the vicinity of the eigen oscillations intersection, then the longitudinal wave number imaginary part, located in the narrow region, increases steeply. This fact is associated with zero reversion of such oscillation group velocity that usually determines the gain. In this case, the spatial increment is determined by the wave frequency major derivatives over the longitudinal wave number. As it follows from the comparison of Fig. 2 and Fig. 3, the presence of plasma in the transit channel brings about a 10 % broadening in the amplification band with the concomitant gain increasing by about 10 %.

Fig. 4 shows plots of the maximum gain and the frequency, corresponding to this maximum value, as a function of plasma density. In the frequency range under investigation the gain increases almost linearly

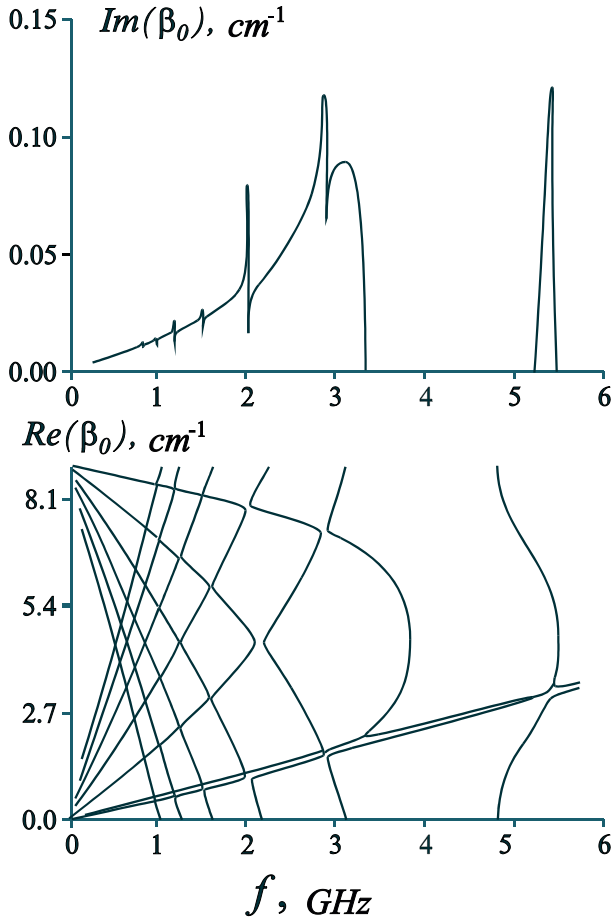


Fig. 3. Real ($Re\beta_0$) and imaginary ($Im\beta_0$) parts of the longitudinal wave number for the beam-running plasma-filled coaxial SWS as a function of frequency. Structure and beam parameters are the same as in Fig. 2, the plasma density being $n_p = 1.8 \cdot 10^{11} \text{ cm}^{-3}$.

with increasing plasma density. This behavior of the gain can, in all evidence, be explained by the linear growth of the beam-carrying resonance wave with increasing plasma density and decreasing its group velocity.

As follows from the expressions (7), (10), the cable wave longitudinal electric field transverse structure, to which e-beam is coupled, is anti-symmetrical for the zero spatial harmonic. As a consequence, the gain must tend to zero when the e-beam radius is precisely compatible with zero position of the longitudinal electric field. This observation is evident from Fig. 5, in which the relationships are shown of the maximum gain vs. beam radius for the first and second pass bands. In the second pass band, the gain increases monotonously during e-beam displacement from the inner transit channel boundary to the outer.

An important parameter, characterizing the slow-wave system performances, is the wave resistance that is determined in the microwave electronics in the

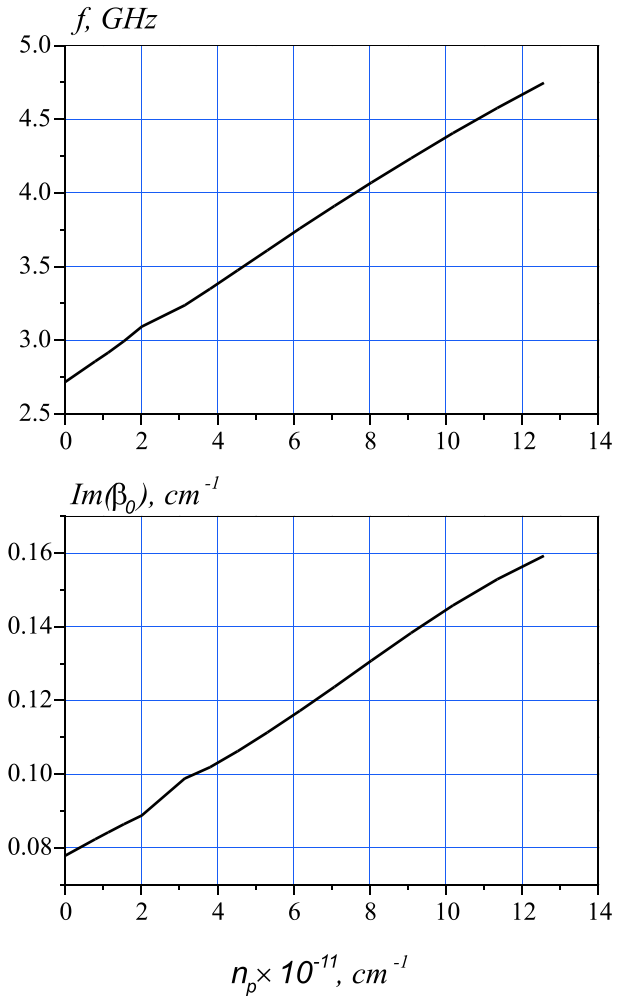


Fig. 4. Maximum gain and wave frequency, corresponding to this maximum, as a function of plasma density. Structure and beam parameters are the same as in Fig. 2.

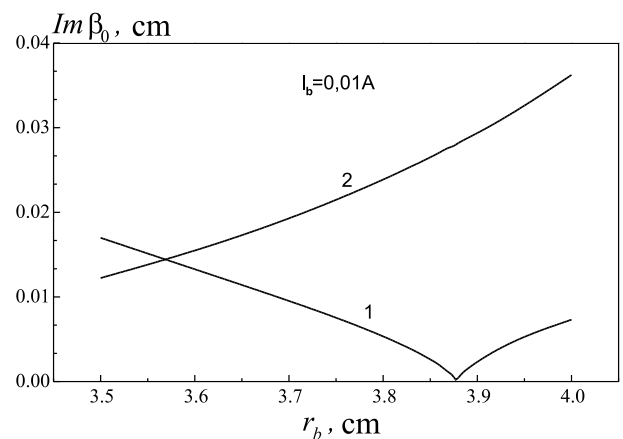


Fig. 5. Maximum gain in the first (1) and second (2) transparency bands as a function of the beam radius. Structure parameters are the same as in Fig. 2.

following way [12]:

$$\rho_w = \left| \int_1^2 \vec{E} d\vec{l} \right| / 2P_z, \quad (19)$$

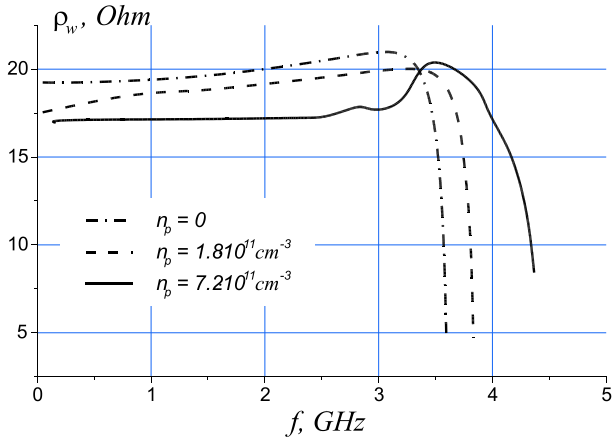


Fig. 6. Wave resistance of coaxial SWS as a function of frequency for different plasma densities. Structure parameters are the same as in Fig. 2.

wherein the contour integral is computed in-between the points on the transmission line conductive surfaces that are found in the system transverse cross-section plane, P_z is the longitudinal energy flow in the slow-wave system. Relative to our case, the wave resistance design formula has the following form:

$$\rho_w = 60 \left| \int_{\sigma}^a E_r^{II} dr \right|^2 / \int_{\sigma}^a E_r^{II} H_{\varphi}^{II*} r dr \text{ (Ohm)}. \quad (20)$$

Fig. 6 shows the relationships of slow-wave transmission line wave resistance vs. frequency for different plasma densities. As it follows from the above plots, the wave resistance varies weakly during plasma filling, that is to say it remains nearly constant in the main pass band. Owing to the dispersion linear section broadening, the wave resistance varies weakly across a larger frequency interval so it does in the vacuum case. That is to say that the possibility of a good SWS matching with devices of microwave power input or output across a broad frequency range still stands a good chance during plasma filling.

3. Non-Linear Operation Mode

In order to study the non-linear stage of e-beam interaction with eigen waves in the coaxial slow-wave transmission line, we will forge ahead, based on the equation for the transverse cross-section-averaged, longitudinal electric field amplitude E [15,16]:

$$\frac{dE}{dz} + i(\beta_e - \beta_0)E = \beta_0^2 I_b R_c^0 \frac{1}{2\pi} \int_0^{2\pi} \exp(i\theta) d\theta \quad (21)$$

and the beam particle motion equations:

$$\frac{dv(z)}{dz} = \frac{e}{mv(z)} \left(1 - \frac{v^2(z)}{c^2} \right)^{3/2} \text{Re} (E e^{-i\theta}), \quad (22)$$

$$\frac{d\theta}{dz} = \beta_e \left(\frac{v_0}{v(z)} - 1 \right).$$

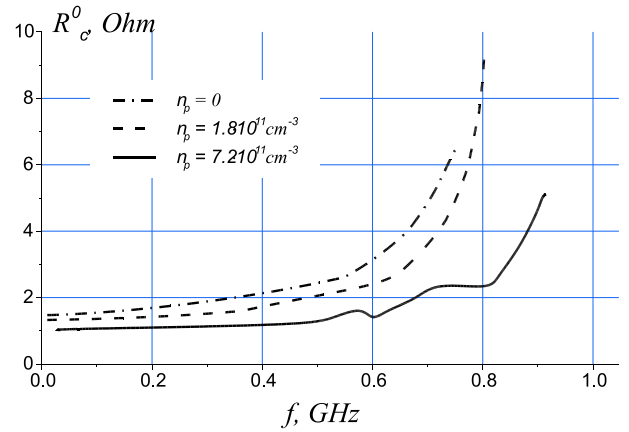


Fig. 7. Coaxial SWS coupling impedance as a function of frequency for different plasma densities. Structure parameters are the same as in Fig. 2.

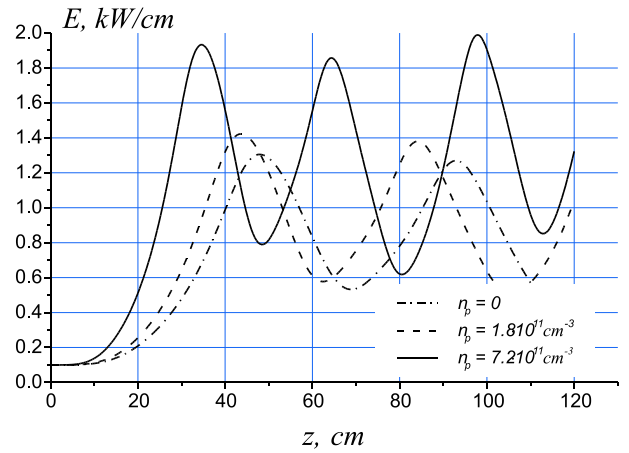


Fig. 8. Longitudinal electric field amplitude as a function of the structure length for some plasma densities. Structure and beam parameters are the same as in Fig. 2.

In the equations (21)-(22), the following designations are used: $\beta_e = \omega/v_0$, ω and β – the wave frequency and longitudinal wave number, I_b – the beam current, v – the speed of beam electrons. The coupling impedance R_c^0 is determined in the following way [15,16]:

$$R_c^0 = \frac{|E_{z,0}^{II}(r_b)|^2}{\frac{c}{2\pi} \beta_0^2 \sum_{m=-\infty}^{\infty} \int_S E_{r,m}^{II} H_{\varphi,m}^{II*} dS}, \quad (23)$$

where S – the transit channel transverse cross-section, r_b – the e-beam radius, $E_{z,m}^{II}$, $E_{r,m}^{II}$, $H_{\varphi,m}^{II}$ – the electromagnetic field components (7)-(12) of the hybrid structure eigen wave in the absence of the beam ($\alpha_m = 0$).

Figs. 7-10 show results of a numeric solution for the equation set (21)-(23). To perform the numeric simulations, the parameters given above of the

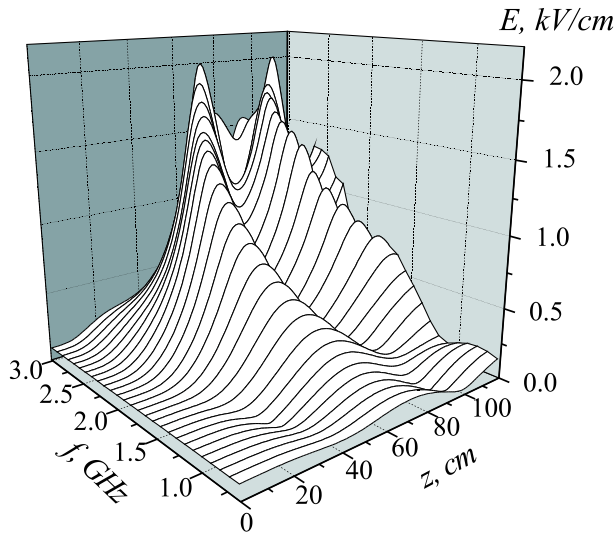


Fig. 9. Longitudinal electric field amplitude vs. wave frequency and coaxial vacuum amplifier length. Structure and beam parameters are the same as in Fig. 2.

experimental facility [11] are used. The beam current is $I_b = 5.0$ A, the energy of beam electrons being $W_b = 35$ keV. Fig. 7 shows the relationships of coupling impedance for the plasma densities $n_p = 1.8 \cdot 10^{11} \text{ cm}^{-3}$ and $n_p = 7.2 \cdot 10^{11} \text{ cm}^{-3}$ vs. frequency. As compared to the vacuum case, the coupling impedance for the plasma-filled slow-wave transmission line remains somewhat lower over a considerable portion of the frequency range, but the maximum coupling impedance value for the plasma-filled version is higher than in the case of the vacuum SWS. This coupling impedance-vs.-frequency relationship coincides with the gain-vs.-frequency relationship (Fig. 2, Fig. 3). The plasma-filled SWS gain is also a little lower over a considerable portion of the frequency range, but its amplification band itself is broader and the maximum gain value greater than for the vacuum structure.

Fig. 8 shows the relationships of longitudinal electric field amplitude-vs.-SWS length. The frequency and wave vector in each case correspond to the maximum gain in the linear operation mode. If the plasma density is $1.8 \cdot 10^{11} \text{ cm}^{-3}$, the longitudinal electric field saturation amplitude is 1.42 KV/cm at the optimum structure length 43.6 cm. For the plasma density the saturation amplitude is 1.93 KV/cm, with the optimum hybrid structure length being 34.8 cm. In the vacuum case, the similar characteristics are 1.3 KV and 48 cm. The coupling efficiency relationships indicate that the maximum e-beam energy losses are approximately the same for the vacuum and plasma-filled coaxial SWS, constituting 24-26 %. The optimum length (at maximum losses) of the plasma-filled structure is considerably shorter, for all that. In this way, the non-linear analysis supports the assumption, put forward while doing

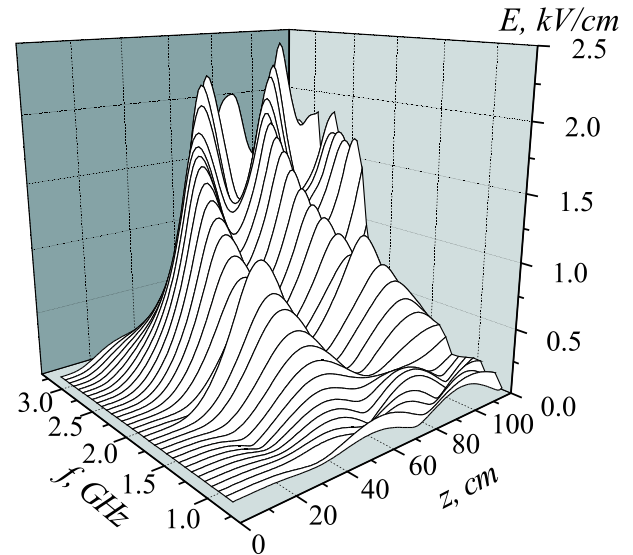


Fig. 10. Longitudinal electric field amplitude vs. wave frequency and plasma coaxial amplifier length. Structure and beam parameters are the same as in Fig. 2, the plasma density being $n_p = 1.8 \cdot 10^{11} \text{ cm}^{-3}$.

the linear analysis, to the point that the principal effect of plasma filling is reduced to the shifting of resonance interactions into the region of higher frequencies. What is said is related, of course, to such problem formulation, in which this particular problem is solved. Namely, the wave frequency is not fixed, as done by some authors earlier [2, 6] while considering other hybrid structures, but amplification of all possible frequencies is considered in the pass band. The resonance frequency increases naturally at that with increasing plasma density.

The family of relationships of longitudinal electric field vs. structure length is given for different eigen frequencies in Fig. 9 for the vacuum structure and in Fig. 10 for plasma-filled ($n_p = 1.8 \cdot 10^{11} \text{ cm}^{-3}$) structures. The first amplitude peak-vs.-frequency relationship corresponds to the gain-vs.-frequency one (Fig. 2, Fig. 3), with the optimum SWS length varying weakly in its pass band. Non-linear computer simulations support the linear theory conclusions about excited frequency band broadening and gain increasing as a result of filling the vacuum SWS interacting channel with plasma.

4. Conclusions

Studies on the electro-dynamic characteristics of the plasma-filled coaxial slow-wave transmission line indicate that it shows much promise for creating high-power microwave devices. During filling of the vacuum coaxial SWS with plasma it retains its wideband features. Moreover, the gain increases and amplification bandwidth broadens, as compared to the vacuum case. The gain-vs.-plasma density relationship

has the linear character in the first pass band of the structure. Principal e-beam interaction occurs with the slow T -wave. The plasma modes, corresponding to eigen oscillations of the tubular plasma column where the beam propagates, are excited weakly. Their amplification bandwidth is small. The wave resistance of the SWS depends weakly on frequency in the first pass band, while the frequency range, in which it is constant, even widens during plasma-filling. The non-linear numeric simulations indicate that the maximum wave saturation amplitudes are higher in the plasma-filled SWS than in the vacuum case. The optimum lengths of the plasma-filled coaxial SWS are shorter by far than those of the vacuum structure. The relationship of saturation amplitude and interaction efficiency vs. frequency has a similar nature with the gain-vs.-frequency relationship. Note that in the meantime the amplitude of saturation and coupling efficiency has a peak in the proximity of beam resonance with the SWS eigen wave and drops down to the low frequency region.

Acknowledgements The Author is grateful to Dr. E.A. Kornilov for useful discussions and thanks are due to Dr. P.I. Markov for his invaluable assistance in performing the calculations.

This work was partially supported by STCU Grant N 256.

Manuscript revised December 1, 2000.

References

- [1] Fainberg Ya.B., Bliokh Yu.P., Kornilov E.A., et al. Electrodynamics of hybrid plasma waveguiding slow down structures // *Doklady AN Ukr.SSR. Phys.-Math and Tech. Sci.* - 1990. - N 11. - P. 55-58.
- [2] Fainberg Ya.B., Bliokh Yu.P., Lubarsky M.G., et al. Electrodynamics hybrid slowing structures // *Fizyka Plasmy.* - 1994. - V 20. - P. 757-766.
- [3] Antonov A.N., Bliokh Yu.P., Degtyar' Yu.A., et al. Beam-plasma generator based on e-beam interaction with plasma waveguiding structures bounded by inductive coupled cavities chains // *Fizyka Plasmy.* - 1994. - V 20. - P. 777-781.
- [4] Zavyalov M.A., Martynov V.O., Mitin L.A., et al. High power beam-plasma UHF amplifier // *IX Symp. on High-Current Electronics. Abstracts. Russia.* - 1992. - P. 132-133.
- [5] Carmel Y., Miami K., Kohs R.A. et al. Demonstration of efficiency enhancement in high-power backward-wave oscillator by plasma injection // *Phys. Rev. Lett.* - 1989. - V. 62. - P. 2389-2392.
- [6] Kornilov E.O., Korostelyov O.M., Lodygin O.V. et al. Electrodynamics hybrid slow down structure kind of irised coaxial line filled by plasma // *UFZh.* - 1995. - V. 40. - P. 312-317.
- [7] Kornilov E.A., Markov P.I., Sotnikov G.V. Excitation of broadband oscillations by electron beam in coaxial slowing transmission line // *Proc. 7th Int. Crimean Conf on Microwave Engineering & Telecommunication Technologies.* - 1997. - V 2. - P. 427.
- [8] Kornilov E.A., Markov P.I., Sotnikov G.V. Excitation of broadband oscillations by electron beam in coaxial disk loaded transmission line // *Proc. of 12th Int. Conf. on High Power Particle Beams "Beams'98".* - V. 1. - P. 877-880.
- [9] Sotnikov G.V. Excitation of broadband oscillations by electron beam in coaxial slow down transmission line // *Electromagnetic Phenomena.* - 1998. - V. 1, N 3. - P. 383-393.
- [10] Stel'makh M.F., Ol'derogge E.B. Electromagnetic wave propagation in irised slow down systems having circular slots // *Radio-Engineering & Electronics.* - 1959. - V 4. - P. 980-987.
- [11] Antipov V.S., Karpukhin B.I., Kornilov E.A., Loginov L.A. A microwave generator with a hybrid coaxial slow-wave structure and a plasma emitter // *Proc. 8th Int. Crimean Conf. On Microwave Engineering & Telecommunication Technologies. Proc.* - 1998. - V. 2. - P. 749-750.
- [12] Grigor'ev A.D., Yankevich V.B. Cavities and Cavity-Based Slow-Wave Structures in the Microwave -M.: Radio and Communications. - 1984. - 248 p.
- [13] Sylin R.A., Sazonov V.P. Slow-Wave Structures - M.: Sov. Radio. - 1966. - 632 p.
- [14] Freud H.P., Zaidman E.G., Antonsen T.M. Theory of helix travelling wave tubes with dielectric and vane loading // *Phys. Plasmas.* - 1996. - V. 3, No. 8. - P. 3145-3165.
- [15] Weinstein L.A., Solntzev V.A. Lectures in Ultra-High Frequency Electronics - M.: Sov. Radio. - 1973. - 400 p.
- [16] Grigor'ev A.D. Electrodynamics & Microwave Technologies - M.: Vyschshaya Schkola Publishers. - 1990. - 335 p.